Research Article | Vol. 30, No. 14 / 4 Jul 2022 / Optics Express 24544

Optics EXPRESS

Accurate optical optimization of light-emitting diodes with consideration of coupling between Purcell factor and transmittance coefficient

SIYUAN HUANG,[1] YONGPIN CHEN,[2] YANG (MICHAEL) YANG,[1,4] AND WEI E. I. SHA[3,5]

[1]State Key Laboratory of Modern Optical Instrumentation, College of Optical Science and Engineering, Zhejiang University, Hangzhou, Zhejiang, 310027, China
[2]School of Electronic Science and Engineering, University of Electronic Science and Technology of China, Chengdu, Sichuan, 611731, China
[3]Key Laboratory of Micro-Nano Electronic Devices and Smart Systems of Zhejiang Province, College of Information Science and Electronic Engineering, Zhejiang University, Hangzhou, Zhejiang, 310027, China
[4]yangyang15@zju.edu.cn
[5]weisha@zju.edu.cn

Abstract: The calculation method for light emission efficiency splits external quantum efficiency (EQE) into internal quantum efficiency (IQE) and light extraction efficiency (LEE) independently. Consequently, the IQE connected to Purcell factor and the LEE are calculated separately. This traditional method ignores the interplays between the Purcell factor and transmittance coefficient in spectral domain, which all strongly depend on emitting directions. In this work, we propose a new figure of merit to describe the light emission process accurately by using the direction-dependent Purcell factor and transmittance coefficient simultaneously. We use a specific LED structure as a numerical example to illustrate the calculation method and optimization procedure.

1. Introduction

Optical loss has always been one of the core issues in designing high-performance light emitting diodes (LEDs). The transfer-matrix method is always adopted to analyze the proportion of energy that couples to the far-field. The optical loss is originated from two parts, including material absorption and waveguide modes. By using transfer-matrix method, researchers optimize the thickness of each layer to maximize light emission, thereby the optimal device structure is obtained. However, this calculation process has an unphysical assumption that the change of the device structure will not modify the luminescence of the emission layer. In fact, due to the Purcell effect, the spontaneous emission of the quantum emitters in the emission layer will be significantly modified when the optical environment is changed. Therefore, the Purcell factor must be considered in the analysis of the light emission process [1]. The calculation of the Purcell effect in LEDs has been developed in literature [2–8]. The external quantum efficiency (EQE) was split into internal quantum efficiency (IQE) and light extraction efficiency (LEE) independently, i.e.:

$$\eta_{EQE} = \eta_{IQE} * \eta_{LEE} \tag{1}$$

Purcell effect changes the spontaneous emission rate and thus changes the internal quantum efficiency as:

$$\eta_{IQE} = \frac{F_p * \eta_0}{(F_p - 1) * \eta_0 + 1} \tag{2}$$

Here, F_p is the Purcell factor, and η_0 is the primitive internal quantum efficiency. η_{LEE} is calculated based on the device structure [2–8]. This calculation method ignores a fact that both the Purcell factor and transmission coefficient depend on transverse wavevectors or emitting

#462536 https://doi.org/10.1364/OE.462536
Journal © 2022 Received 28 Apr 2022; revised 1 Jun 2022; accepted 15 Jun 2022; published 22 Jun 2022

Optics EXPRESS

directions. In other words, only the Purcell factor and the transmission coefficient averaged in all directions were calculated in literature. Therefore, the "averaged" Purcell factor may not be properly used in the internal quantum efficiency, as well as the "averaged" transmission coefficient in the calculation of light extraction efficiency. The coupling between the direction-dependent Purcell factor and transmission coefficient should be taken into account. Hence, a more accurate expression describing the light emission process is given by:

$$CE(z) = \int S(\omega)d\omega \sum_{\sigma} \int F_p^{\sigma}(k_\rho, \omega, z)T^{\sigma}(k_\rho, \omega, z)dk_\rho \tag{3}$$

Here, k_ρ, z and ω are the transverse wave-vectors, location of recombination centers (quantum emitters) and angular frequency respectively. $CE(z)$ counts the enhancement of photons that are detectable in far field. $S(\omega)$ is the luminescence spectrum normalized by intensity maximum of bare bulk material of the emission layer. Moreover, $F_p^{\sigma}(k_\rho, \omega, z)$ is the direction-dependent Purcell factor; and $T^{\sigma}(k_\rho, \omega, z)$ is the direction-dependent transmission coefficient. σ represents the polarization TE or TM. Formula (3) shows the interplay between the Purcell factor and transmission coefficient in the spectral domain (wavenumber space). $CE(z)$ is a figure of merit for device optimization which reveals the real light emission process. The following content of this article consists of two parts. The first is the derivation of CE, then a LED structure is used as a numerical example to illustrate the analysis procedure.

2. Results and discussion

2.1. Derivation of CE

The LED model can be simplified to multilayer planar medium, so what we need to do is to get the direction-dependent Purcell factor and transmission coefficient of this structure. From the Fermi golden rule:

$$\gamma = \frac{2\pi}{\hbar}\Sigma_f |<f|\hat{H}_I|i>|^2 \delta(\omega_f - \omega_i) \tag{4}$$

we can get the conclusion that the spontaneous emission rate is proportional to the imaginary part of the trace of the dyadic Green's Function with $\boldsymbol{r}_0$ as both the source point and the observation point [9]:

$$\gamma(\boldsymbol{r_0}, \omega) \propto \mathrm{Im}[Tr\{\bar{\boldsymbol{G}}(\boldsymbol{r_0}, \boldsymbol{r_0}, \omega)\}] \tag{5}$$

The route of derivation is to get the dyadic Green's function with an arbitrary source point and observation point first, and then let the observation point be in the position of source point. Based on this idea, in the beginning, we obtain the expression of dyadic Green's function expanded in the spectral domain. Since TE and TM modes are decoupled in multilayer planar medium, the dyadic Green's function can be written as:

$$\bar{\boldsymbol{G}}(\boldsymbol{r}, \boldsymbol{r}', \omega) = \bar{\boldsymbol{G}}^{TE}(\boldsymbol{r}, \boldsymbol{r}', \omega) + \frac{1}{k_m^2}\bar{\boldsymbol{G}}^{TM}(\boldsymbol{r}, \boldsymbol{r}', \omega) \tag{6}$$

Here, $k_m = k_0^2 \epsilon_m \mu_m$ is the wave-vector and m is the ordinal number of the layer where the source point is. (see Fig. 1)In the above formula, $\bar{\boldsymbol{G}}^{TE}$ and $\bar{\boldsymbol{G}}^{TM}$ are:

$$\bar{\boldsymbol{G}}^{TE}(\boldsymbol{r}, \boldsymbol{r}', \omega) = (\nabla \times \hat{z})(\nabla' \times \hat{z})g^{TE}(\boldsymbol{r}, \boldsymbol{r}', \omega) \tag{7}$$

$$\bar{\boldsymbol{G}}^{TM}(\boldsymbol{r}, \boldsymbol{r}', \omega) = (\nabla \times \nabla \times \hat{z})(\nabla' \times \nabla' \times \hat{z})g^{TM}(\boldsymbol{r}, \boldsymbol{r}', \omega) \tag{8}$$

where $g^{\sigma}(\boldsymbol{r}, \boldsymbol{r}', \omega)$ ($\sigma = TE\ or\ TM$) is:

$$g^{\sigma}(\boldsymbol{r}, \boldsymbol{r}', \omega) = \frac{i}{4\pi}\int_0^{\infty} \frac{dk_\rho}{k_{mz}k_\rho} J_0(k_\rho \rho) F^{\sigma}(k_\rho, \omega, z, z') \tag{9}$$

Optics EXPRESS

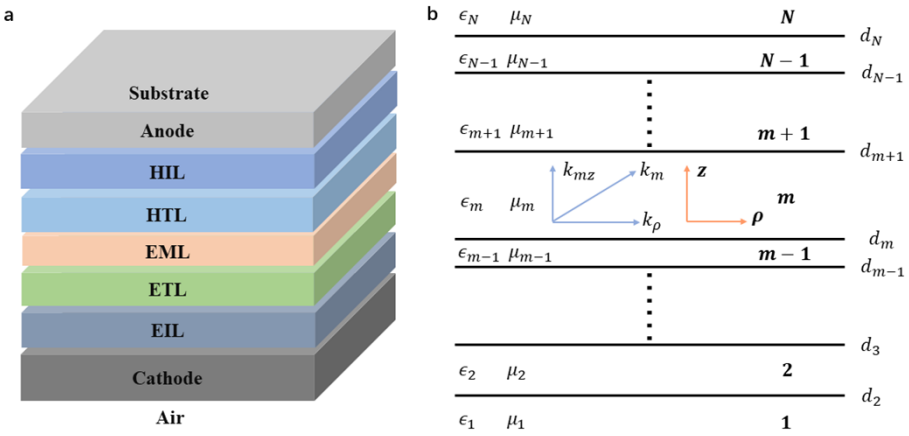

Fig. 1. **a.** General device structure of ultra-thin LEDs; **b.** Multilayer planar medium structure as a simplified model of LEDs.

Here, $F^{\sigma}(k_\rho, \omega, z, z')$ is the propagation factor has been given in Ref. [10] and attached in the appendix A. $J_0(k_\rho \rho)$ is the Bessel function. Substituting (9) into (7) and (8), we can get the expressions of the dyadic Green's Function. What we are interested with is the diagonal terms which relate to the local density of state (LDOS). The six diagonal terms are attached in appendix B [11]. Based on this, we can easily get the trace:

$$Tr\{\bar{\boldsymbol{G}}^{TE}(\boldsymbol{r}, \boldsymbol{r}', \omega)\} = \frac{i}{4\pi}\int_0^{\infty} dk_\rho \frac{F^{TE}(k_\rho, \omega, z, z')}{k_{mz}} J_0(k_\rho \rho) k_\rho \tag{10}$$

$$Tr\{\bar{\boldsymbol{G}}^{TM}(\boldsymbol{r}, \boldsymbol{r}', \omega)\} = \frac{i}{4\pi}\int_0^{\infty} dk_\rho \frac{(\partial_z \partial_{z'} + k_\rho^2) F^{TM}(k_\rho, \omega, z, z')}{k_{mz}} J_0(k_\rho \rho) k_\rho \tag{11}$$

Here, $(\partial_z \partial_{z'} + k_\rho^2) F^{TM}(k_\rho, \omega, z, z')$ is attached in appendix A. Let $\boldsymbol{r} = \boldsymbol{r}' = \boldsymbol{r}_0$, then $J_0(k_\rho \rho) = 1$, finally we can get the transverse wavevector related $Im[Tr\{\bar{\boldsymbol{G}}^{TE}(\boldsymbol{r}_0, \boldsymbol{r}_0, \omega)\}]$ and $Im[Tr\{\bar{\boldsymbol{G}}^{TM}(\boldsymbol{r}_0, \boldsymbol{r}_0, \omega)\}]$. Based on this, we can obtain the wavevector (direction) dependent spontaneous emission rate and thus direction-dependent Purcell factor, by dividing the spontaneous emission rate in the inhomogeneous environment to that in the vacuum [12]:

$$F_p^{TE}(k_\rho, \omega, z) = Re\{F^{TE}(k_\rho, \omega, z)\} \tag{12}$$

$$F_p^{TM}(k_\rho, \omega, z) = Re\{\frac{1}{k_m^2}(\partial_z \partial_{z'} + k_\rho^2) F^{TM}(k_\rho, \omega, z)\} \tag{13}$$

Here, $F^{TE}(k_\rho, \omega, z)$ and $(\partial_z \partial_{z'} + k_\rho^2) F^{TM}(k_\rho, \omega, z)$ are:

$$F^{TE}(k_\rho, \omega, z) = \frac{[1 + \tilde{R}^{TE}_{m,m+1} e^{2ik_{mz}(d_{m+1} - z)}][1 + \tilde{R}^{TE}_{m,m-1} e^{2ik_{mz}(z - d_m)}]}{1 - \tilde{R}^{TE}_{m,m-1} \tilde{R}^{TE}_{m,m+1} e^{2ik_{mz}(d_{m+1} - d_m)}} \tag{14}$$

$$\begin{aligned} \frac{1}{k_m^2}(\partial_z \partial_{z'} + k_\rho^2) F^{TM}(k_\rho, \omega, z) = & \frac{1 + \tilde{R}^{TM}_{m,m-1} \tilde{R}^{TM}_{m,m+1} e^{2ik_{mz}(d_{m+1} - d_m)}}{1 - \tilde{R}^{TM}_{m,m-1} \tilde{R}^{TM}_{m,m+1} e^{2ik_{mz}(d_{m+1} - d_m)}} \\ & + \frac{(k_\rho^2 - k_{mz}^2)[\tilde{R}^{TM}_{m,m+1} e^{2ik_{mz}(d_{m+1} - z)} + \tilde{R}^{TM}_{m,m-1} e^{2ik_{mz}(z - d_m)}]}{k_m^2 (1 - \tilde{R}^{TM}_{m,m-1} \tilde{R}^{TM}_{m,m+1} e^{2ik_{mz}(d_{m+1} - d_m)})} \end{aligned} \tag{15}$$

So far, we get the direction-dependent Purcell factor. Meanwhile the direction-dependent transmittance coefficient has actually been given in this calculation procedure:

$$T^{\sigma}(k_\rho, \omega, z) = 1 - |\tilde{R}^{\sigma}_{m,m+1}|^2 \tag{16}$$

Optics EXPRESS

Here we need to note that the transverse wavevector k_ρ represents the emission angle when k_ρ is within a certain range. The normalized emission spectrum $S(\omega)$ can be obtained through a measurement experiment and normalization procedure. Finally, we get the analytical expression of $CE(z)$.

2.2. Numerical Examples

Traditional LED devices usually have large thickness. LED based on III-V compound semiconductors, such as GaAs, has a total thickness that reaches one micrometer, and thus the Purcell effect is not obvious. With the development of the LED devices, the trend of thickness reduction has become irresistible. Micro-LEDs, OLEDs that have been commercialized for display, Perovskite LEDs which have become hotspots in recent years, and devices that using 2D materials usually have a total thickness that is less than the emission wavelength. Therefore, the Purcell effect becomes non-negligible. For ultra-thin LED devices such as OLEDs and perovskite LEDs, both electrical and optical properties should be considered together when we set the thickness of each layer. From the perspective of electrical performances, we need to place the recombination centers of electron-hole pairs at the emission layer. Hence the thickness of the electron transport layer and hole transport layer restrict each other. For example, when we decrease the thickness of ETL, the thickness of HTL should also decrease simultaneously to ensure that the recombination centers of electron-hole pairs still fall in the emission layer. Besides, the thicknesses of some layers have certain ranges due to the constraints of fabrication techniques. Consequently, there are a series of geometric constraints in the optimization of optical performance. Under these constraints, the thickness of the emission layer, cathode layer, and anode layer usually have a moderate adjustment range. Here, we use the following device structure of perovskite LEDs from Ref. [13] as an example: Air/ Al(100 nm)/ TPBI(50 nm)/ TBTB(5 nm)/ EML(50 nm)/ HIL(45 nm)/ ITO(70 nm)/ Glass. The complex refractive indexes are 1, 0.68 + 5.3i, 1.73, 1.8, 1.6, 1.43, 1.85, and 1.5 respectively.

Taking the above device structure as an example, we first draw $k_\rho - \omega$ diagrams under different emission layer thickness (the rest of the layers remain unchanged), which are Figs. 2(a-c). These three $k_\rho - \omega$ diagrams draw the product of the direction-dependent Purcell factor and transmittance coefficient under each direction and wavelength. They are similar to the band diagrams of one-dimensional photonic crystals. The difference is that the band diagrams of one-dimensional photonic crystals have clear sharp band edges due to the periodicity of the structure. We know that the physical meaning of the energy band of photonic crystals is not only the permission and prohibition of light propagation, but also the enhancement and suppression of spontaneous emission [14,15]. Although a LED structure does not have sharp band edges, the spontaneous emission rate under different directions and wavelengths will still vary greatly as shown in the Figs. 2(a-c). Hence the strongest emission can be obtained by aligning the emission spectrum of the LED with the enhanced part of the energy band diagram. It should be noted that we cannot only use the Purcell factor to match the emission spectrum, but also need to take the transmittance coefficient into consideration. Because the transmittance coefficient decreases generally while the spontaneous emission is enhanced, resulting in the reduced output light intensity. The competition between the transmittance coefficient and Purcell factor resembles the concept of quality factor (Q) in lasers. A large Q value leads to an improved Purcell factor and enhanced light emission while a small Q value leads to high transmittance. Consequently, there will be a balanced point of Q value to maximize the light output. Based on this, $k_\rho - \omega$ diagram draws the product of the direction-dependent Purcell factor and transmittance coefficient. Subsequently, we can get the CE with λ (see Fig. 2(d)) by taking integration of k_ρ under each λ according to the $k_\rho - \omega$ diagram. Then we can obtain the counts enhancement of detectable photons in the far-field through matching the $CE(\lambda)$ and normalized emission spectrum (Fig. 2(e)). Figure 2(d) shows that $CE(\lambda)$, which λ is within the emission wavelength range, increases first

Optics EXPRESS

and then decreases as the thickness of emission layer increases, so there must be a maximum value of *CE* at a certain thickness of emission layer. Figure 2(f) illustrates that the best thickness of emission layer is 50 nm when other layers remain unchanged.

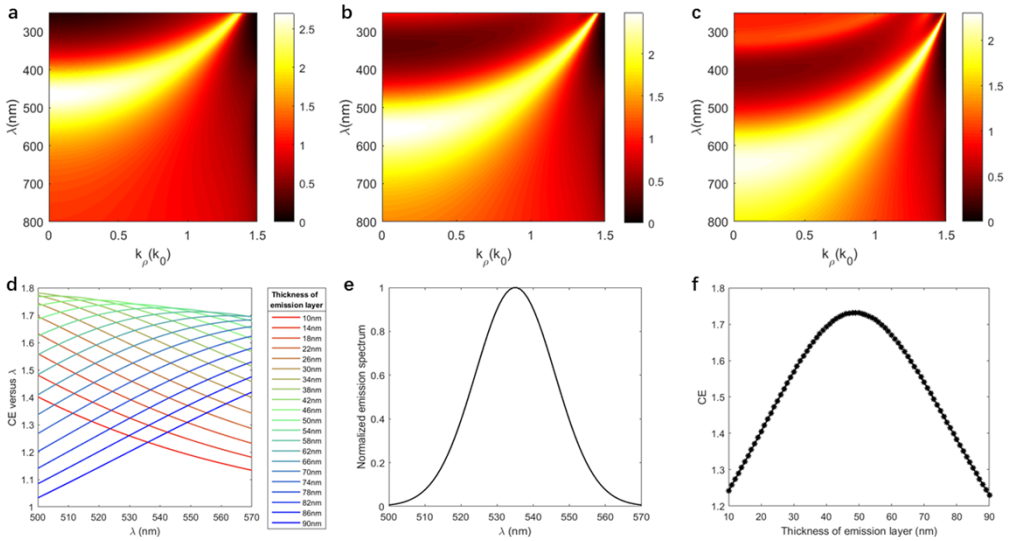

Fig. 2. a-c. The product of direction-dependent Purcell factor and transmittance coefficient at each frequency (ω) and direction (k_ρ) which can be coupled to the far-field. Here the thicknesses of the emission layer are 20 nm, 50 nm and 80 nm for **a**, **b** and **c** respectively. **d.** The product of direction-dependent Purcell factor and transmittance coefficient after taking an integration for all direction (k_ρ) which can be coupled to the far-field. **e.** Normalized emission spectrum of the emission layer. **f.** Counts enhancement of photons that are detectable in far-field under different thickness of the emission layer. All the values of **a**, **b**, **c**, **d** and **f** are averaged for all positions of the emission layer.

The analysis above gives the optimal thickness of emission layer which is consistent with the 50 nm used in the Ref. [13]. Cathode and anode have ignorable effect on the electrical performance of LEDs as long as their thickness are within a certain range, so there is room for optimizing the thickness of the electrodes. We optimize the thickness of ITO layer and metal layer separately while keeping the thickness of other layers unchanged. It can be found from Fig. 3(a) that $CE(\lambda)$ increases first and decreases as the thickness of ITO layer increases. This phenomenon is similar to that with the emission layer as the variable. After matching the $CE(\lambda)$ with the normalized emission spectrum, we find that 85 nm is the best thickness of ITO layer (Fig. 3(b)). Though this data has a slight difference from that in Ref. [13], the value of *CE* only differs by $1.7657/1.7352 - 1 = 2\%$. At the same time, we also optimized the thickness of the cathode (metal) (Fig. 3(c)). The results show that as long as the thickness of the metal is greater than a certain value ($\approx$50 *nm*), the change in its thickness will hardly affect the light emission of the LED (Fig. 3(d)). This conclusion is in line with our experience.

The foregoing analysis has fixed the thickness of other layers. Actually, we can use the thickness of multiple layers as optimized variables under some constraints which ensure high electrical performances. The calculation speed is very fast since the expression is analytic. By using the multivariate nonlinear optimization, we could find the truly optimal structure. Here we use the thickness of ITO and emission layer as variables. No matter the initial condition (thickness of emission layer) is set to 20 nm, 50 nm or 80 nm, it will eventually converge to the same best thickness combination $(ITO, EML) = (99\ nm, 38\ nm)$ after less than 10 iterations. (see Fig. 4) These three optimizations cost 54.69 seconds, 51.97 seconds, and 57.24 seconds respectively. The

Optics EXPRESS

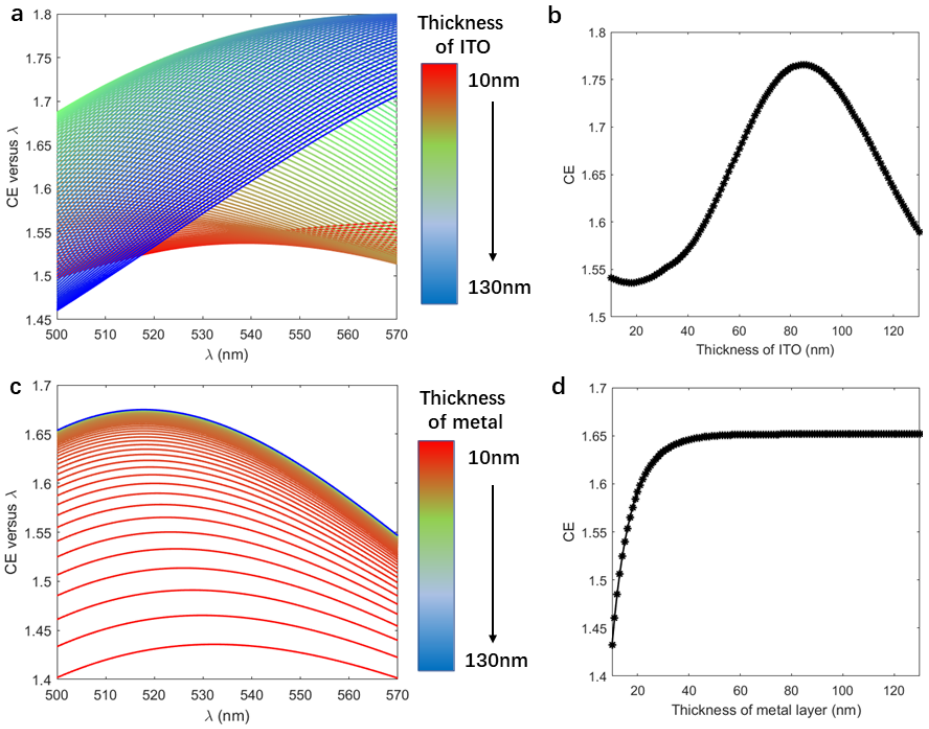

Fig. 3. **a.** The product of direction-dependent Purcell factor and transmittance coefficient after taking an integration for all directions (k_ρ) that can couple to the far-field under different thickness of ITO layer. **b.** Counts enhancement of photons that are detectable in far-field under different thickness of ITO layer. **c-d.** Analogous to **a** and **b** but under different thickness of metallic cathode layer. All the values of **a**, **b**, **c** and **d** are averaged for all positions of the emission layer.

light emission efficiency of this structure is 1.05 times higher than $(ITO, EML) = (70\ nm, 50\ nm)$ which is adopted by Ref. [13]. In the actual optimization problem, we can first get some constraints in view of the needs of the electrical performances, such as the range of each layer and the relations between ETL and HTL. Then we can set up the thickness of each layer as optimized variables to obtain the optimal device structure.

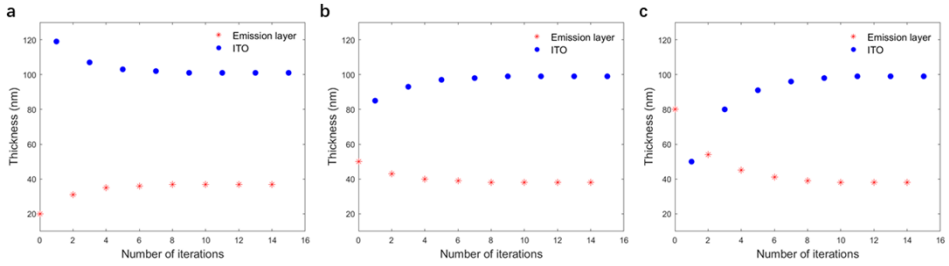

Fig. 4. The iterative process of optimizing the thicknesses of emission layer and ITO layer under different initial thicknesses of emission layer. The thicknesses of emission layer are 20 nm for **a**, 50 nm for **b** and 80 nm for **c**.

Optics EXPRESS

2.3. Comparison with average method

The above numerical example has illustrated how to obtain the optimal device structure by using the direction-dependent Purcell factor and transmittance coefficient. Here, we also calculated the product of the direction-average Purcell factor and transmittance coefficient (Fig. 5(a, b)). The direction-average Purcell factor is a function of only wavelength and position that is obtained by an integration of direction-dependent Purcell factor. The parameters are still set in the same way as the original structure in Ref. [13], only changing the thickness of the emission layer. The calculation results show a significant difference compared to Fig. 2(d, f). The optimal thickness of the emission layer is 52 nm here while the actual best thickness is 50 nm when the other layers remain unchanged. This obvious difference reveals the necessity of using the directional-dependent Purcell factor and transmittance coefficient.

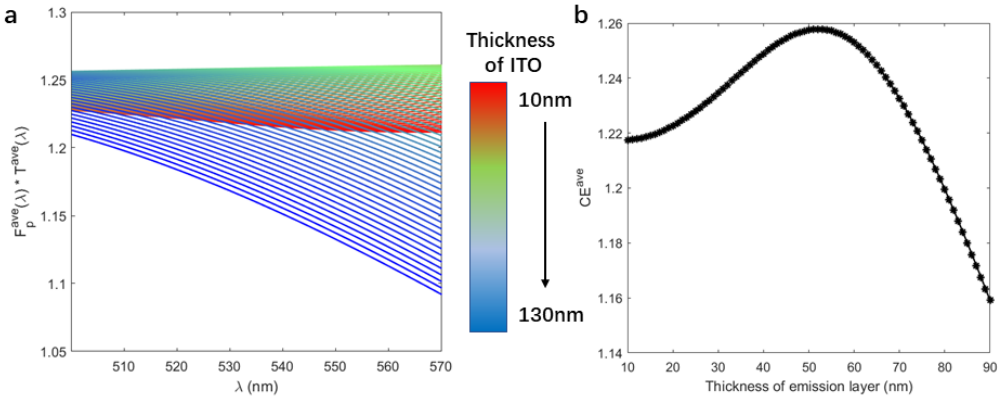

Fig. 5. a. The product of the direction-average Purcell factor and transmittance coefficient under different thickness of emission layer. **b.** Counts enhancement of photons that are detectable in far-field under different thickness of emission layer. All the values of **a** and **b** are averaged for all positions of the emission layer.

3. Conclusion

This article thoroughly clarifies how the Purcell effect affects the light emission process of LEDs. The traditional method did not consider the interplay between the Purcell factor and transmittance coefficient in the spectral domain. In fact, the change of structure affects the LEE, but also affects the spontaneous emission rate, which in turn affects the IQE. Therefore, we cannot separate the LEE and IQE into two independent parts for consideration. This article proposed a figure of merit to accurately describe the light emission process through deriving the analytical expressions of both the direction-dependent Purcell factor and the direction-dependent transmittance coefficient. Besides, we selected a LED structure as an example to illustrate how to calculate the figure of merit and optimize the light emission. Actually, this calculation method is applicable to all light-emitting devices with planar structures, including top-emitting LEDs and resonant-cavity LEDs. For LED devices with non-planar structures, it is necessary to develop numerical Green's function to obtain the direction-dependent Purcell factor, so as to accurately describe the light emission process.

Optics EXPRESS

Appendix

A. Propagation factor

In the case that the source point and the observation point are in the same layer, the propagation factor $F^{\sigma}(k_\rho, \omega, z, z')$ can be represented as:

$$F^{\sigma}(k_\rho,\omega,z,z') = e^{ik_{mz}|z-z'|} + \frac{\tilde{R}^{\sigma}_{m,m-1}e^{ik_{mz}(z+z'-2d_m)} + \tilde{R}^{\sigma}_{m,m+1}e^{ik_{mz}(2d_{m+1}-z-z')}}{1-\tilde{R}^{\sigma}_{m,m-1}\tilde{R}^{\sigma}_{m,m+1}e^{2ik_{mz}(d_{m+1}-d_m)}} + \frac{2\tilde{R}^{\sigma}_{m,m-1}\tilde{R}^{\sigma}_{m,m+1}e^{2ik_{mz}(d_{m+1}-d_m)}\cos[k_{mz}(z-z')]}{1-\tilde{R}^{\sigma}_{m,m-1}\tilde{R}^{\sigma}_{m,m+1}e^{2ik_{mz}(d_{m+1}-d_m)}} \tag{17}$$

Here, k_ρ and k_{mz} are shown in the Fig. 1. They satisfy the relations $k_\rho^2 + k_{mz}^2 = k_m^2$. z and z' are the z coordinate values of the observation point and source point respectively. $\tilde{R}^{\sigma}_{m,m-1}$ and $\tilde{R}^{\sigma}_{m,m+1}$ are the general reflection coefficients which can be calculated by following iterative formula:

$$\tilde{R}^{\sigma}_{i,i+1} = \frac{R^{\sigma}_{i,i+1} + \tilde{R}^{\sigma}_{i+1,i+2}e^{2ik_{i+1,z}(d_{i+2}-d_{i+1})}}{1 + R^{\sigma}_{i,i+1}\tilde{R}^{\sigma}_{i+1,i+2}e^{2ik_{i+1,z}(d_{i+2}-d_{i+1})}} \tag{18}$$

$$\tilde{R}^{\sigma}_{i,i-1} = \frac{R^{\sigma}_{i,i-1} + \tilde{R}^{\sigma}_{i-1,i-2}e^{2ik_{i-1,z}(d_{i}-d_{i-1})}}{1 + R^{\sigma}_{i,i-1}\tilde{R}^{\sigma}_{i-1,i-2}e^{2ik_{i-1,z}(d_{i}-d_{i-1})}} \tag{19}$$

where $R^{\sigma}_{i,i+1}$ and $R^{\sigma}_{i,i+1}$ are Fresnel formula. The boundary conditions for these two iterations process is $\tilde{R}^{\sigma}_{N,N+1} = 0$ for formula (18) and $\tilde{R}^{\sigma}_{1,0} = 0$ for formula (19) respectively. $(\partial_z\partial_{z'} + k_\rho^2)F^{TM}(k_\rho, \omega, z, z')$ should also be given:

$$(\partial_z\partial_{z'} + k_\rho^2)F^{TM}(k_\rho,\omega,z,z') = k_m^2 e^{ik_{mz}|z-z'|} + \frac{(k_\rho^2-k_{mz}^2)[\tilde{R}^{\sigma}_{m,m-1}e^{ik_{mz}(z+z'-2d_m)} + \tilde{R}^{\sigma}_{m,m+1}e^{ik_{mz}(2d_{m+1}-z-z')}]}{1-\tilde{R}^{\sigma}_{m,m-1}\tilde{R}^{\sigma}_{m,m+1}e^{2ik_{mz}(d_{m+1}-d_m)}} + \frac{2k_m^2\tilde{R}^{\sigma}_{m,m-1}\tilde{R}^{\sigma}_{m,m+1}e^{2ik_{mz}(d_{m+1}-d_m)}\cos[k_{mz}(z-z')]}{1-\tilde{R}^{\sigma}_{m,m-1}\tilde{R}^{\sigma}_{m,m+1}e^{2ik_{mz}(d_{m+1}-d_m)}} \tag{20}$$

B. Diagonal terms of dyadic Green's function

By substituting formula (9) into formula (7) and (8), The diagonal terms of dyadic Green's Function $\bar{\boldsymbol{G}}^{TE}$ and $\bar{\boldsymbol{G}}^{TM}$ can be represented as:

$$G^{TE}_{xx} = \frac{i}{2\rho}\cos(2\phi)S_1\left\{\frac{F^{TE}}{k_{mz}k_\rho^2}\right\} + \frac{i}{4}(1-\cos(2\phi))S_0\left\{\frac{F^{TE}}{k_{mz}}\right\} \tag{21}$$

$$G^{TE}_{yy} = -\frac{i}{2\rho}\cos(2\phi)S_1\left\{\frac{F^{TE}}{k_{mz}k_\rho^2}\right\} + \frac{i}{4}(1+\cos(2\phi))S_0\left\{\frac{F^{TE}}{k_{mz}}\right\} \tag{22}$$

$$G^{TE}_{zz} = 0 \tag{23}$$

$$G^{TM}_{xx} = -\frac{i}{2\rho}\cos(2\phi)S_1\left\{\frac{\partial_z\partial_{z'}F^{TM}}{k_{mz}k_\rho^2}\right\} + \frac{i}{4}(1+\cos(2\phi))S_0\left\{\frac{\partial_z\partial_{z'}F^{TM}}{k_{mz}}\right\} \tag{24}$$

$$G^{TM}_{yy} = \frac{i}{2\rho}\cos(2\phi)S_1\left\{\frac{\partial_z\partial_{z'}F^{TM}}{k_{mz}k_\rho^2}\right\} + \frac{i}{4}(1-\cos(2\phi))S_0\left\{\frac{\partial_z\partial_{z'}F^{TM}}{k_{mz}}\right\} \tag{25}$$

$$G^{TM}_{zz} = \frac{i}{2}S_0\left\{\frac{k_\rho^2F^{TM}}{k_{mz}}\right\} \tag{26}$$

Optics EXPRESS

Here, ρ and ϕ are polar coordinates. $S_n\{f\}$ is an integral formula:

$$S_n\{f\} = \frac{1}{2\pi}\int_0^\infty dk_\rho \cdot f \cdot J_n(k_\rho\rho)\cdot k_\rho^{n+1} \tag{27}$$

Formula (10) and (11) can be obtained by adding (21) ~ (23) and (24) ~ (26) respectively.

Funding. National Natural Science Foundation of China (61975177, U20A20164).

Disclosures. The authors declare no conflict of interest.

Data availability. Data underlying the results presented in this paper are not publicly available at this time but may be obtained from the authors upon reasonable request.

References

1. E. M. Purcell, "Spontaneous emission probabilities at radio frequencies," Phys. Rev. **69**(1-2), 37–38 (1946).
2. Y. D. Zheng, F. A. Xiao, W. J. Liu, and X. L. Hu, "Purcell effect and light extraction of Tamm-plasmon-cavity green light-emitting diodes," Opt. Express **27**(21), 30852–30863 (2019).
3. H. Cho, J. Chung, J. Song, J. Lee, H. Lee, J. Lee, J. Moon, S. Yoo, and N. S. Cho, "Importance of Purcell factor for optimizing structure of organic light-emitting diodes," Opt. Express **27**(8), 11057–11068 (2019).
4. S. K. Kim, S. W. Jung, H.-U. Park, R. Lampande, and J. H. Kwon, "Accurate optical simulation method of tandem organic light-emitting diode with consideration of Purcell effect," Org. Electron. **95**, 106192 (2021).
5. M. Kovacic, D. Samigullina, F. Bouchard, J. Krc, B. Lipovsek, M. Soldera, A. F. Lasagni, S. Reineke, and M. Topic, "Analysis and optimization of light outcoupling in OLEDs with external hierarchical textures," Opt. Express **29**(15), 23701–23716 (2021).
6. K. A. Neyts, "Simulation of light emission from thin-film microcavities," J. Opt. Soc. Am. A **15**(4), 962–971 (1998).
7. H.-Y. Ryu, "Modification of internal quantum efficiency and efficiency droop in GaN-based flip-chip light-emitting diodes via the Purcell effect," Opt. Express **23**(19), A1157–A1166 (2015).
8. E. F. Schubert, N. E. J. Hunt, M. Micovic, R. J. Malik, D. L. Sivco, A. Y. Cho, and G. J. Zydzik, "Highly Efficient Light-Emitting Diodes with Microcavities," Science **265**(5174), 943–945 (1994).
9. L. Novotny, B. Hecht, and O. Keller, "Principle of Nano-Optics," Phys. Today **60**, 62 (2006).
10. W. C. Chew, "*Waves and Fields in Inhomogenous Media*," Wiley-IEEE Press (1990).
11. Y. P. Chen, W. C. Chew, and L. Jiang, "A New Green's Function Formulation for Modeling Homogeneous Objects in Layered Medium," IEEE Trans. Antennas Propagat. **60**(10), 4766–4776 (2012).
12. Y. P. Chen, W. E. I. Sha, W. C. H. Choy, L. Jiang, and W. C. Chew, "Study on spontaneous emission in complex multilayered plasmonic system via surface integral equation approach with layered medium Green's function," Opt. Express **20**(18), 20210–20221 (2012).
13. Y.-H. Kim, S. Kim, A. Kakekhani, J. Park, J. Park, Y.-H. Lee, H. Xu, S. Nagane, R. B. Wexler, D.-H. Kim, S. H. Jo, L. Martínez-Sarti, P. Tan, A. Sadhanala, G.-S. Park, Y.-W. Kim, B. Hu, H. J. Bolink, S. Yoo, R. H. Friend, A. M. Rappe, and T.-W. Lee, "Comprehensive defect suppression in perovskite nanocrystals for high-efficiency light-emitting diodes," Nat. Photonics **15**(2), 148–155 (2021).
14. Y. a. Eli, "Inhibited Spontaneous Emission in Solid-State Physics and Electronics," Phys. Rev. Lett. **58**(20), 2059–2062 (1987).
15. D. Kleppner, "Inhibited Spontaneous Emission," Phys. Rev. Lett. **47**(4), 233–236 (1981).